Citation: Khalifa, A., Çakir, Z., Owen, L.A., Kaya, Ş., 2019. Evaluation of the Relative Tectonic Activity of the Adıyaman fault within the Arabian-Anatolian plate boundary (eastern Turkey). *Geologica Acta, 17.6, 1-17.*
DOI: 10.1344/GeologicaActa2019.17.6

geologica acta

Evaluation of the Relative Tectonic Activity of the Adıyaman fault within the Arabian-Anatolian plate boundary (eastern Turkey)

A. Khalifa[1, 2] Z. Çakir[1] L.A. Owen[2] Ş. Kaya[3]

[1]Department of Geological Engineering, Faculty of Mines, Istanbul Technical University
Maslak, 34467 Sarıyer/Istanbul, Turkey. Khalifa E-mail: akhalifa@itu.edu.tr

[2]Department of Geology, University of Cincinnati
Cincinnati, OH 45221, USA

[3]Department of Geomatics, Faculty of Civil Engineering, Istanbul Technical University
Maslak, 34467 Sarıyer/Istanbul, Turkey

ABSTRACT

The left-lateral strike-slip Adıyaman fault is located in eastern Turkey within the plate boundary deformation zone between Arabia and Anatolia. The Adıyaman fault is a major splay from the East Anatolian Fault (EAF), one of the most important tectonic structures in the Eastern Mediterranean region. These faults are consequence of the collision between the Arabian and Anatolian plates and the resulting westward tectonic escape of Anatolia. Although the EAF has been intensively studied since its discovery in the late 1960s, little is known about the Adıyaman fault and its tectonic activity. In this study, we extract geomorphic indices including mountain-front sinuosity (S_{mf}), valley floor width-to-height ratio (V_f), stream length-gradient (S_L), catchment Asymmetry Factor (AF) and hypsometric integrals and curves (HI and HC) to evaluate the relative tectonic activity of the Adıyaman fault. These three geomorphic indices (AF, HI, and HC) are averaged to define an index for Relative Tectonic Activity (RTA) that allows the Adıyaman fault to be divided into categories of low, moderate and high RTA. The results confirm that the Adıyaman fault is an active fault with high to moderate Quaternary tectonic activity. However, this fault is of minor importance on accommodating plate boundary deformation, as evidenced by the recent crustal motions determined by GPS studies. Nevertheless, it is worthwhile to note that the Adıyaman fault still poses a significant seismic hazard for the region despite its relatively moderate tectonic activity.

KEYWORDS | **Tectonic geomorphology. Geomorphic indices. Adıyaman strike-slip fault. Eastern Turkey.**

INTRODUCTION

Deformation within tectonically active areas is mostly examined and determined using geomorphic, geodetic and geologic data (Dumont *et al.*, 2005; Molin *et al.*, 2004; Necea *et al.*, 2005). Recent tectonic activity along faults that are associated with continental deformation has given rise to varied tectonic landforms and landscapes (Giamboni *et al.*, 2005; Gordon, 1998). Geomorphic indices are useful tools to assess the tectonic activity/deformation along active faults, allowing sections of the fault to be dividing into

stretches of Relative Tectonic Activity (RTA) (Bull and McFadden, 1977; Rockwell *et al.*, 1984). Geomorphic analyses have previously been successfully applied to many tectonically active areas, including Central America (Wells *et al.*, 1988), California (USA), (Lifton and Chase, 1992), southern Italy (Molin *et al.*, 2004), southern Spain (Pérez-Peña *et al.*, 2010), eastern North America (Frank *et al.*, 2011), western Pakistan (Ul-Hadi *et al.*, 2013), northern Turkey (Selim *et al.*, 2013), Central Anatolia, Turkey (Yıldırım, 2014) and eastern Turkey (Khalifa *et al.*, 2018; Matoš *et al.*, 2016; Selçuk, 2016). We examine the Adıyaman fault in eastern Turkey to provide insights into the geomorphic development along active faults and, neotectonics in Anatolia. The Adıyaman fault is a left-lateral strike-slip fault located in the continental East Anatolian Fault (EAF) zone. The Adıyaman fault was mapped by Aksoy *et al.* (2007), but few studies have been undertaken along it despite being an ideal area to examine the RTA/uplift within a continental transform setting. We apply quantitative geomorphometric methods to assess its tectonic activity and to examine how deformation varies along its length. Ultimately, our research will aid in the evaluation of the Adıyaman fault for seismic hazard mitigation and as a guide for future active tectonic studies.

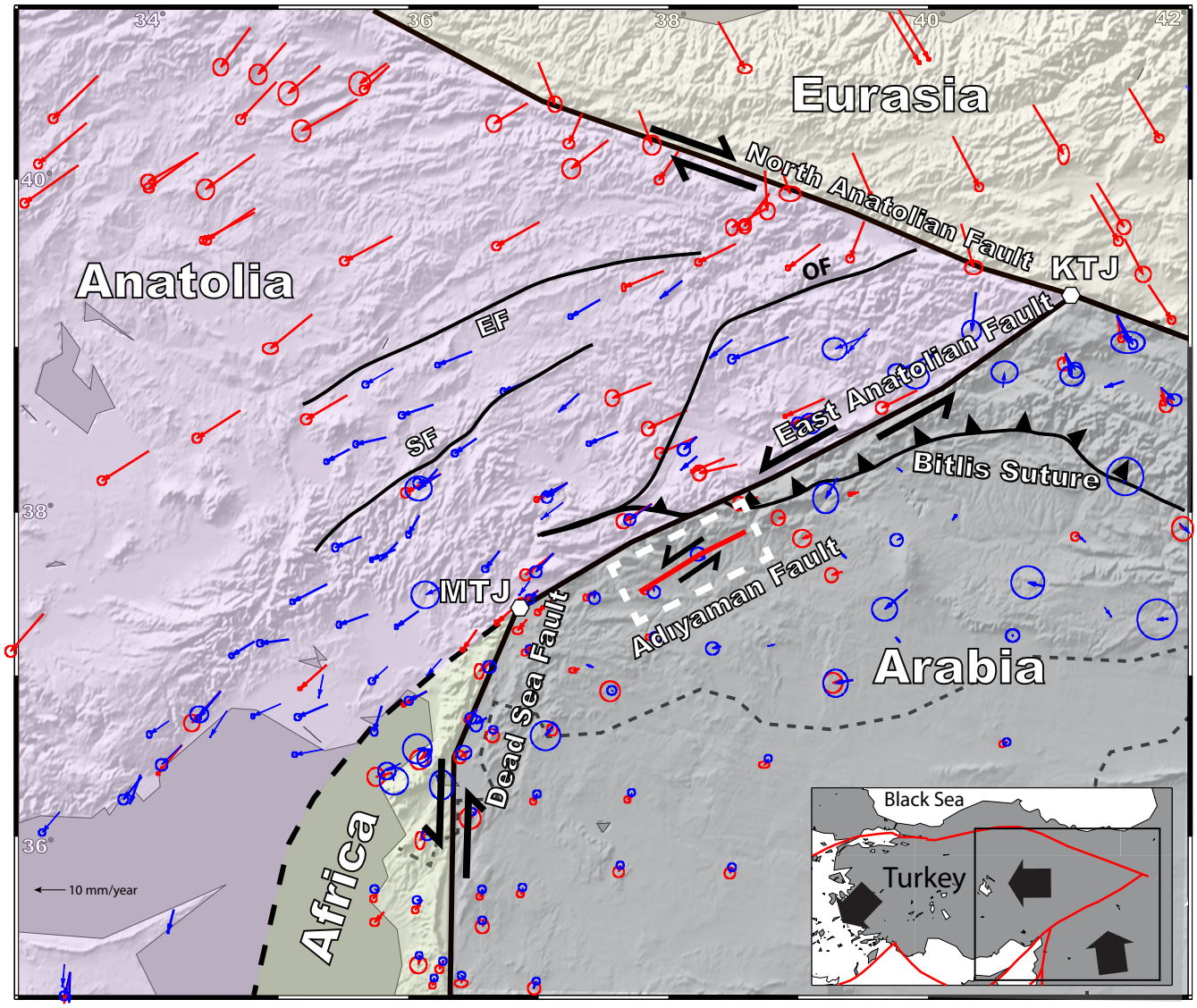

FIGURE 1. Shaded relief image (data from 30m Shuttle Radar Topography Mission (SRTM); Farr *et al.*, 2007) of eastern Turkey showing the African, Arabian, Anatolian and Eurasian plates and major active faults (thick black lines). The Adıyaman fault is shown by a thick red line. Red and blue arrows indicate GPS velocities with respect to a fixed Arabian lithospheric plate, and blue and red circles indicate GPS measurement errors, according to Reilinger *et al.* (2006) and Aktuğ *et al.* (2016), respectively. The inset map and box with white dashed lines show the location of the study area and Figure 2, respectively. EF: Ecemiş Fault; KTJ: Karliova Triple Junction; MTJ: Maraş Triple Junction; OF: Ovacık Fault; SF: Savrun Fault.

REGIONAL SETTING OF THE STUDY AREA

Eastern Anatolia is a province characterized by a N-S compressional tectonic regime (Fig. 1). Conjugate dextral and sinistral strike-slip faults that run sub/parallel to the North and East Anatolian fault zones are the most significant structural features in the region (Bozkurt, 2001). Many of the faults in the eastern Anatolian region are seismically active and they have been the source of numerous destructive earthquakes, *e.g.* the September 13, 1924 Pesinler (M_s=6.8), October 30, 1983 Horasan-Norman (M_s= 6.8), June 6, 1986 Doğanşehir (M_s=5.6) and March 2, 2017 Adıyaman-Samsat (M_w=5.5) (Ambraseys, 1989; Barka et al, 1983; Canıtez and Üçer, 1967; Eyidoğan *et al.*, 1999; McKenzie, 1972; Taymaz *et al.*, 1991; Toksöz *et al.*, 1983) earthquakes.

The EAF was first described by Allen (1969) who showed that it forms part of the transform boundary between the Anatolian and Eurasian, and the African and Arabian lithospheric plates. A series of faults run sub/parallel or oblique to the main trend of the EAF zone (Hempton, 1987; Şaroğlu *et al.*, 1992; Şengör *et al.*, 1985; Taymaz *et al.*, 1991; Westaway, 1994). Views on the timing of initiation of the EAF range from Late Miocene to Early Pliocene (Arpat and Şaroğlu, 1972; Dewey *et al.*, 1986; Hempton, 1987; Perinçek and Çemen, 1990; Şengör *et al.*, 1985). Extending ~75km in ~65ºNE direction, the Adıyaman fault is one of the faults that are parallel to the main EAF zone (Figs. 1; 2). The seismic record associated with the Adıyaman fault is characterized by low to moderate frequency of relatively small to moderate magnitude (M_w=3.0–5.5) earthquakes. The M_w=5.5 Adıyaman-Samsat earthquake was the largest recorded on the fault and occurred at 14:07 (local time) on March 2, 2017 (Fig. 3). Major rock types along the Adıyaman fault zone include Plio-Quaternary undifferentiated continental clastic and carbonate rocks, Middle-Upper Miocene continental clastic rocks, and Upper Cretaceous ophiolitic mélange rocks (Fig. 4). The age of the Adıyaman fault is poorly constrained, Şengör *et al.* (1985) and Dewey *et al.* (1986) suggested that the fault could have been initiated during the Late Miocene to Early Pliocene at the same time as the EAF. The total displacement of the Adıyaman fault is not known.

METHODS

We divide the Adıyaman fault into seven segments on the basis of changes in the trend of the fault trace (Fig. 5). Mountain-front sinuosity (S_{mf}), valley floor width-to-height ratio (V_f), and stream length-gradient (S_L) were calculated for each of the seven segments. Geomorphic indices including catchment Asymmetry Factor (AF), basin hypsometric integral (HI) and hypsometric curves (HC) were calculated for the 39 catchments that cover the entire fault. All the catchments and streams were extracted from the 30m resolution Digital Elevation Model (DEM) of the Shuttle Radar Topography Mission (SRTM) data (Farr *et al.*, 2007), and from Google Earth™ satellite images.

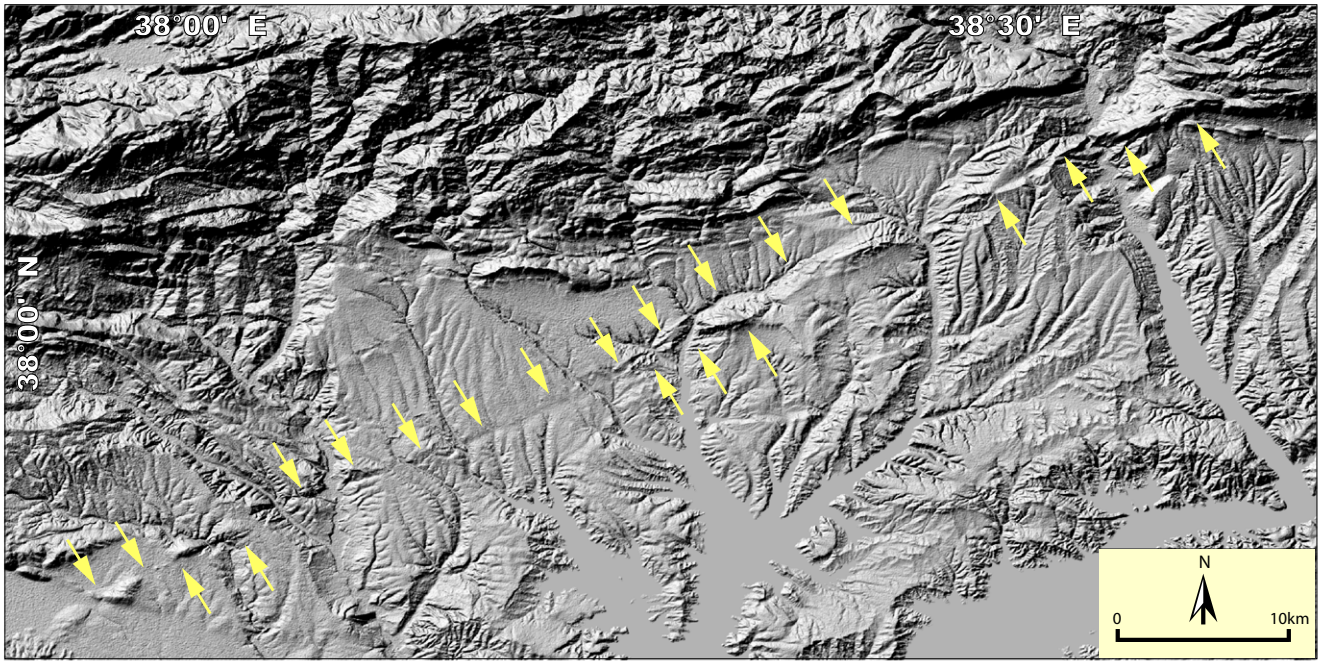

FIGURE 2. Shaded relief image showing the trace of the Adıyaman fault indicated by yellow arrows (data from 30m SRTM; Farr *et al.*, 2007).

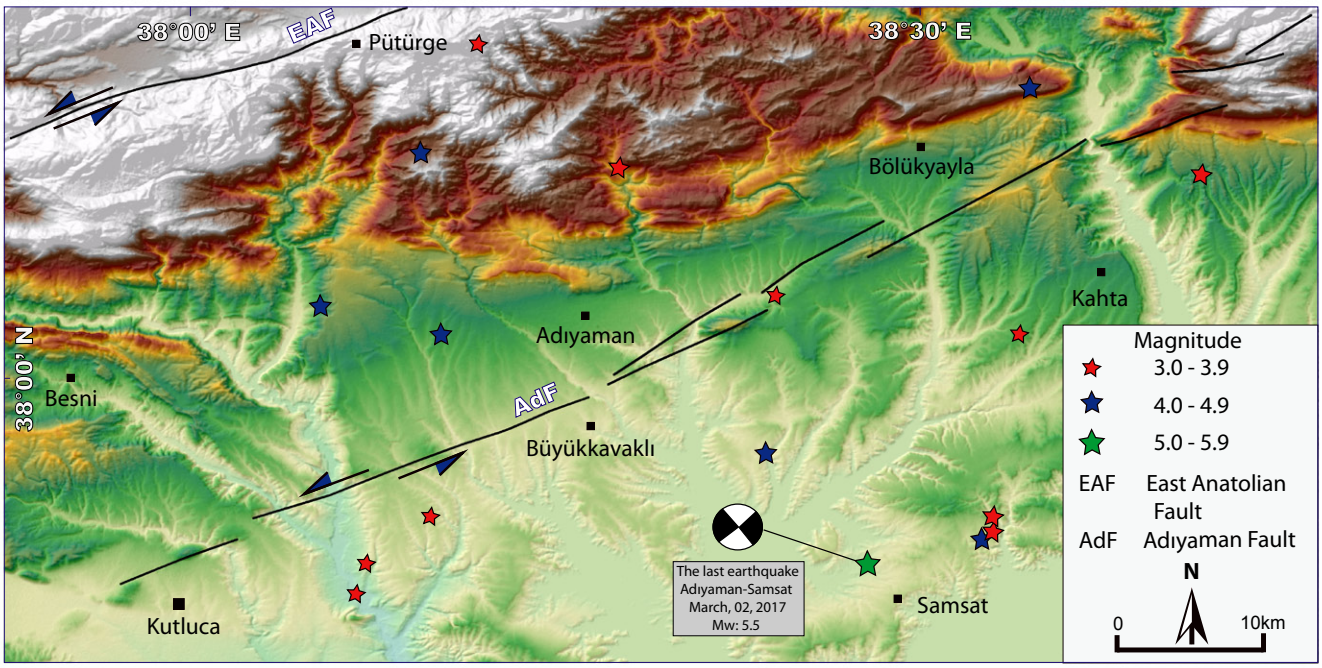

FIGURE 3. Seismotectonic of the study area. Digital Elevation Model (DEM) was generated from 30m SRTM data available at http://srtm.csi.cgiar.org. AdF: Adıyaman Fault; EAF: East Anatolian Fault.

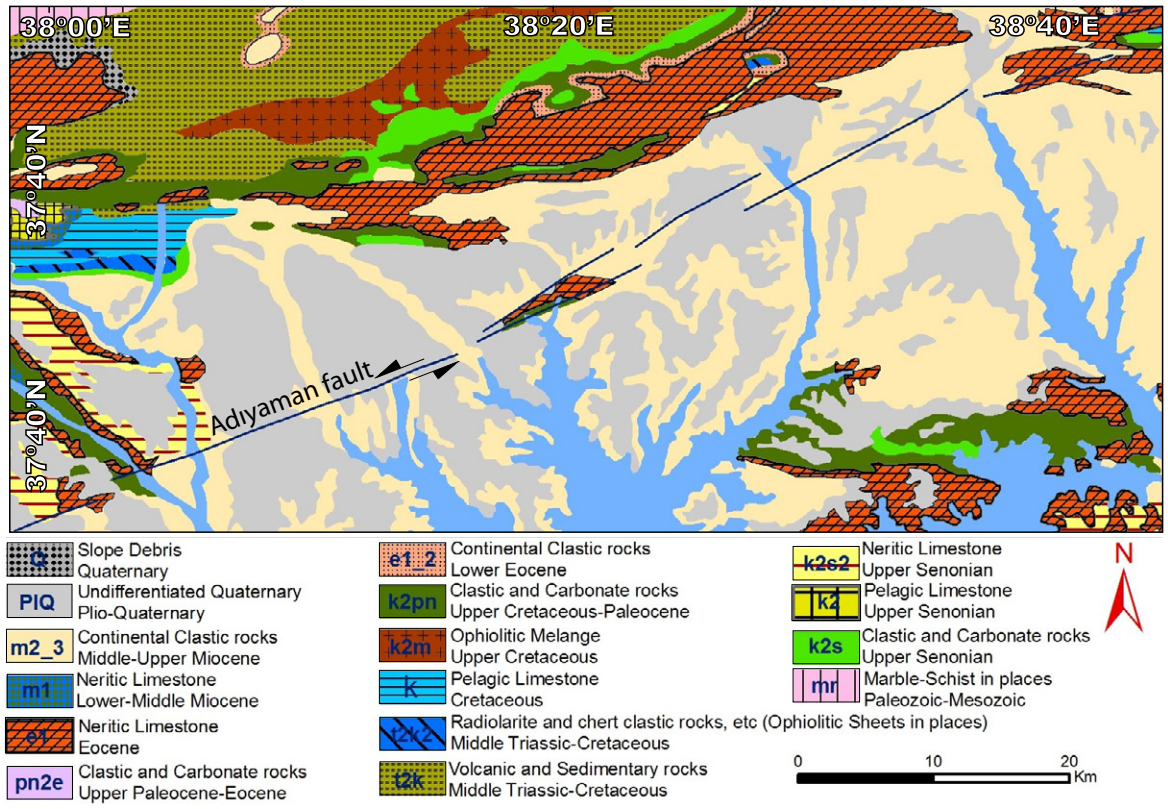

FIGURE 4. Geological map of the Adıyaman fault zone and adjacent areas (from Herece, 2008).

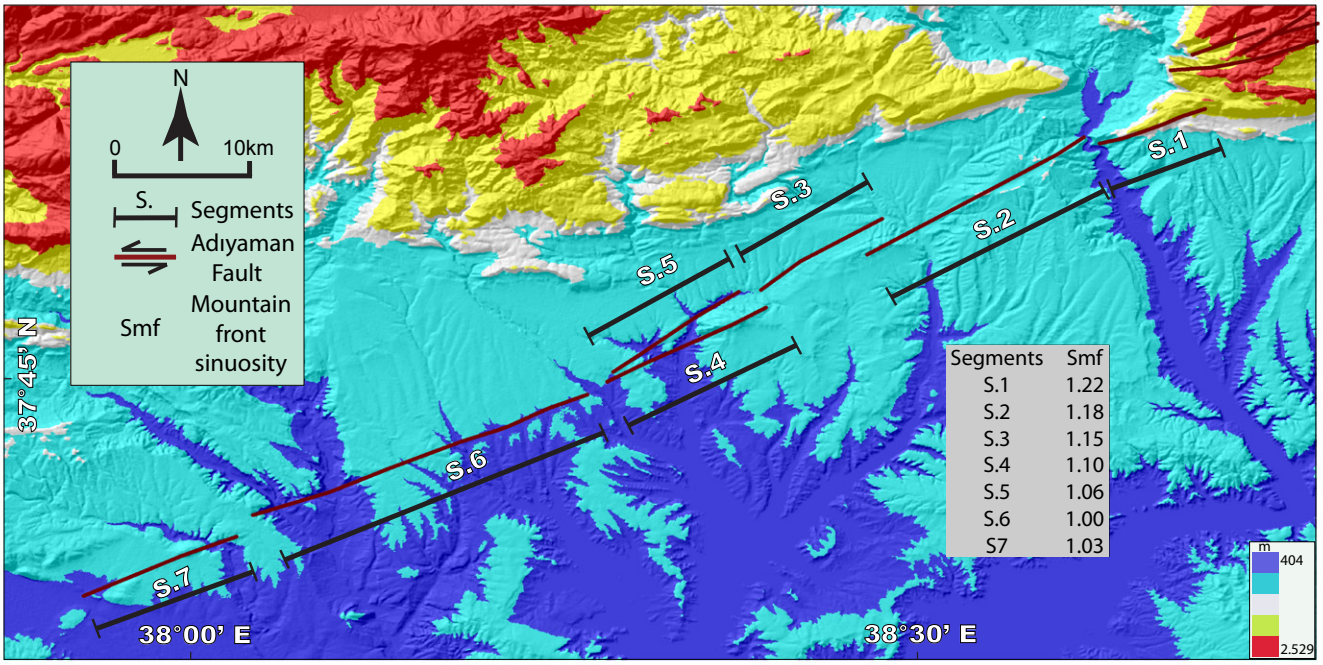

FIGURE 5. Segments of the Adıyaman fault zone. Digital Elevation Model (DEM) generated from 30m SRTM data.

Many studies have used a combination of S_{mf} and V_f to provide a semi-quantitative assessment of the relative degree of tectonic activity along mountain fronts (Selçuk, 2016; Yıldırım, 2014). A plot of S_{mf} against V_f was used to define three different classes of RTA, high, moderate and low (Bull and McFadden, 1977; Silva *et al.*, 2003). Rockwell *et al.* (1984) suggested that S_{mf} values <1.4 and V_f values approaching 1 indicate mountain segments tectonically highly active.

Mountain-front sinuosity (S_{mf})

The S_{mf} index examines the balance between the tendency of erosion to produce an irregular or sinuous mountain front and the tendency active tectonics/faulting to create uplift and a relatively straight mountain front (Bull and McFadden, 1977; Tsodoulos *et al.*, 2008). Bull and McFadden (1977) defined S_{mf} as:

$$S_{mf}=L_{mf}/L_s \quad (1)$$

where L_s is the straight-line length of the mountain front and L_{mf} is the length of the mountain front along the mountain-piedmont junction (Rockwell *et al.*, 1984). Values of S_{mf}, close to 1.0 reflect relative straight mountain fronts associated with high tectonic activity, whereas higher S_{mf} values (>3.0) indicate mountain fronts that are modified by erosion and are relatively tectonically quiescent (Bull, 2007; Pérez-Peña *et al.*, 2010; Silva *et al.*, 2003). In this study, we calculated the S_{mf} index for the seven segments defined along the Adıyaman fault.

Valley floor width-to-height ratio (V_f)

The V_f index is very useful in evaluating the relative rate of incision in areas of uplift. Vf values discriminate between V-shaped valleys, associated with rapid uplift and high incision, and flat-floored valleys. (Azor *et al.*, 2002; El Hamdouni *et al.*, 2008; Keller and Printer, 2002; Silva *et al.*, 2003). Bull and McFadden (1977) defined V_f as:

$$V_f=2V_{fw}/[(E_{ld}-E_{sc})+(E_{rd}-E_{sc})] \quad (2)$$

where V_{fw} is the width of the valley floor, E_{ld} and E_{rd} are the elevations of the left and rightvalley divides, respectively, and E_{sc} is the elevation of the valley floor. In this study, V_f values were calculated for 40 canyons (rivers, streams) along the studied fault zone (Fig. 6).

Stream length-gradient (S_L)

The S_L index was applied by Hack (1973) to examine the impact of rock resistance in streams channels in the south of United States. This index is very sensitive for evaluating the active faults and their tectonic activity degrees (Alipoor *et al.*, 2011; El Hamdouni *et al.*, 2008; Keller and Printer, 2002; Yıldırım, 2014). The S_L index is defined as:

$$S_L=(\Delta h/\Delta t)l \quad (3)$$

where $(\Delta h/\Delta t)$ is the local slope of the stream segment and l is the stream length from the drainage

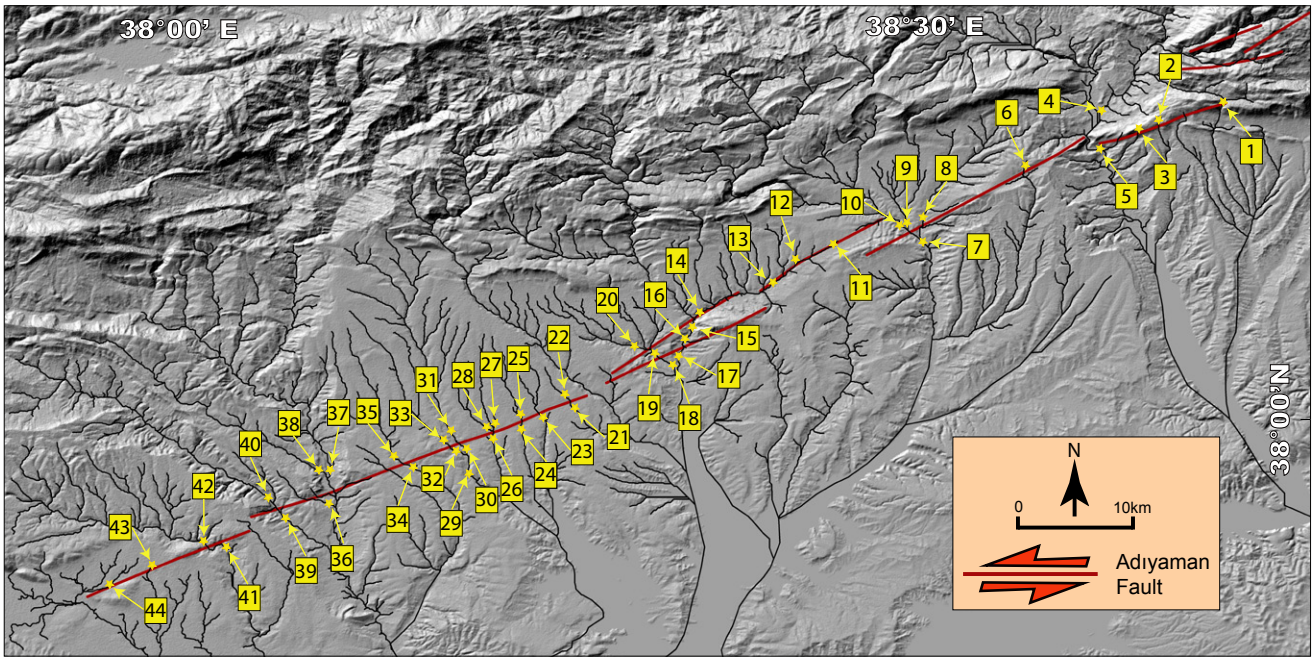

FIGURE 6. Values of valley floor width-to-height ratio (V_f) along the study fault zone.

divide to the midpoint of the stream reach for which the S_L is evaluated (Hack, 1973). S_L were calculated every 50m-along the stream channels. S_L values increase as streams and rivers go through active uplifts and may give lesser values when flowing parallel to valleys produced by strike-slip faults (Keller and Printer, 2002; Yıldırım, 2014). To discuss the S_L index, different classes of rock resistance were defined from very low, low, moderate, high, and very high strength.

Asymmetry Factor (AF)

The AF of a catchment is calculated to detect tectonic tilting at the whole range scale and was defined by Hare and Gardner (1985) and Pérez-Peña *et al.* (2010) as:

$$AF=100(A_r/A_t) \quad (4)$$

where A_t is the catchment area to the right of the main trunk stream and A_r is the drainage area of the whole catchment. If the catchment is symmetric, AF should be ~50 reflecting little or no tilting, whereas higher or lower AF values indicate that the catchment shows a high degree of tilting. AF values include the AF-50, which is the difference between the neutral value of 50 and the measured values (El Hamdouni *et al.*, 2008). For the evaluation of the RTA Perez-Peña *et al.* (2010), Giaconia *et al.* (2012) and Selçuk (2016) defined four classes of asymmetry: symmetric (AF-50<5), gently asymmetric (AF-50 of 5–10), moderately asymmetric (AF-50 of 10–15), and strongly asymmetric (AF-50>15). In our study, the AF was calculated to 39 different drainage systems along the Adıyaman fault. We define three classes of asymmetry following El Hamdouni *et al.* (2008) as: i) class 1, with strong asymmetric (AF-50>15); ii) class 2, with intermediate asymmetric (AF-50 of 10–15); and iii) class 3, with low asymmetric (AF-50 of 5–10).

Hypsometric Integral and Curve (HI and HC)

Hypsometric analysis has been widely used in geomorphology and hydrology, particularly in tectonically active areas (Chen *et al.*, 2003; Ciccacci *et al.*, 1992; D'Alessandro *et al.*, 1999; Lifton and Chase, 1992; Ohmori, 1993; Strahler, 1952; Willgoose, 1994; Willgoose and Hancock, 1998). Lifton and Chase (1992), *e.g.* examined the relationship between tectonics and hypsometric analysis in the San Gabriel mountains in California and found a strong correlation between the uplift rate and the hypsometric integral (HI). HI describes the distribution of area and altitude of a given area of a landscape particularly a catchment and is defined as:

$$HI=(E_{mean}-E_{min})/(E_{max}-E_{min}) \quad (5)$$

where E_{mean} is the mean elevation value, E_{max} is the maximum elevation value, and E_{min} is the minimum elevation value.

A hypsometric curve (HC) is the representation of the distribution of area and elevation within the drainage catchment.

From hypsometric analysis we define three classes in our study: i) class 1, a convex HC with HI>0.5; ii) class 2, a S-shaped or straight HC with HI=0.3–0.5; and iii) class 3, a concave HC with HI<0.3. High HI values are related to young active tectonics and low HI values to older landscapes that have been more eroded and less impacted by recent active tectonics (Keller and Pinter, 2002; Mahmood and Gloaguen, 2012; Pérez-Peña *et al.*, 2010). The HI and HC values were calculated for 39 catchments along the Adıyaman fault.

Relative Tectonic Activity (RTA)

Using the methods of El Hamdouni *et al.* (2008), we classified each of the geomorphic indices, AF, HI, and HC, into three classes (1 to 3) and calculated an average class value that we call G_{av}. Using the G_{av} we define three RTA classes: i) class 1 is $0.5<G_{av}<2$ (high tectonic activity); ii) class 2 is $2\leq G_{av}>2.5$ (moderate tectonic activity); and iii) class 3 is $G_{av}\geq 2.5$ (low tectonic activity).

RESULTS

Mountain-front sinuosity (S_{mf})

Values obtained in the mountain-front sinuosity analysis range from 1.22 to 1.00. The highest S_{mf} value (1.22) is recorded along segment 1 (NE) and the lowest value (1.00) in segment 6 (SW). The results confirm that there is a clear decrease in the S_{mf} index values from segment 1 (NE) to 7 (SW) along the examined fault (Table 1; Fig. 5).

Valley floor width-to-weight ratio (V_f)

The V_f index values for the streams along the study fault range from 0.30 to 1.72, indicating that most of the valleys are V-shaped (Table 2; Fig. 6). The mean Vf values gradually decrease from segment 1 to 7 (Table 1; Fig. 7).

Stream length-gradient (S_L)

The S_L values show a variable distribution along the stream channels draining into the fault zone and range from <50 to >200. S_L values gradually increase toward the mountain-front of each segment. In several locations along the fault zone, the distribution of S_L index has anomalously high values on relatively soft rocks. The highest and most anomalous spots of the S_L index are recorded along all the fault segments. Valleys that flow parallel to segments 3, 5, and 6 reflect the lowest values of the S_L index (Fig. 8).

Catchment Asymmetry Factor (AF)

AF values range from 27 to 86 (Table 3; Fig. 9). Along the study fault, catchments 4, 6, 7, 8, 21, 26, 27, 29, 32, and

TABLE 1. Mountain-front sinuosity (S_{mf}) and mean valley floor width-to-height ratio (V_f) values for each fault segment

Segments	S_{mf}	S_{mf} Class	Mean V_f
S.1	1.22	1	0.98
S.2	1.18	1	0.95
S.3	1.15	1	0.90
S.4	1.10	1	0.80
S.5	1.06	1	0.75
S.6	1.00	1	0.64
S.7	1.03	1	0.48

TABLE 2. Valley floor width-to-height ratios (V_f) for the streams along the study fault

Streams No.	V_f	Streams No.	V_f
1	0.85	23	0.76
2	0.99	24	0.66
3	1.35	25	0.68
4	1.08	26	0.45
5	0.63	27	1.72
6	1.11	28	1.10
7	1.10	29	0.59
8	0.46	30	0.35
9	0.80	31	0.53
10	0.30	32	0.59
11	1.30	33	0.55
12	0.51	34	0.57
13	1.30	35	1.28
14	0.79	36	0.72
15	0.52	37	0.57
16	0.95	38	0.52
17	0.80	39	0.59
18	1.22	40	0.71
19	0.76	41	0.30
20	0.71	42	0.61
21	0.50	43	0.53
22	0.59	44	0.49

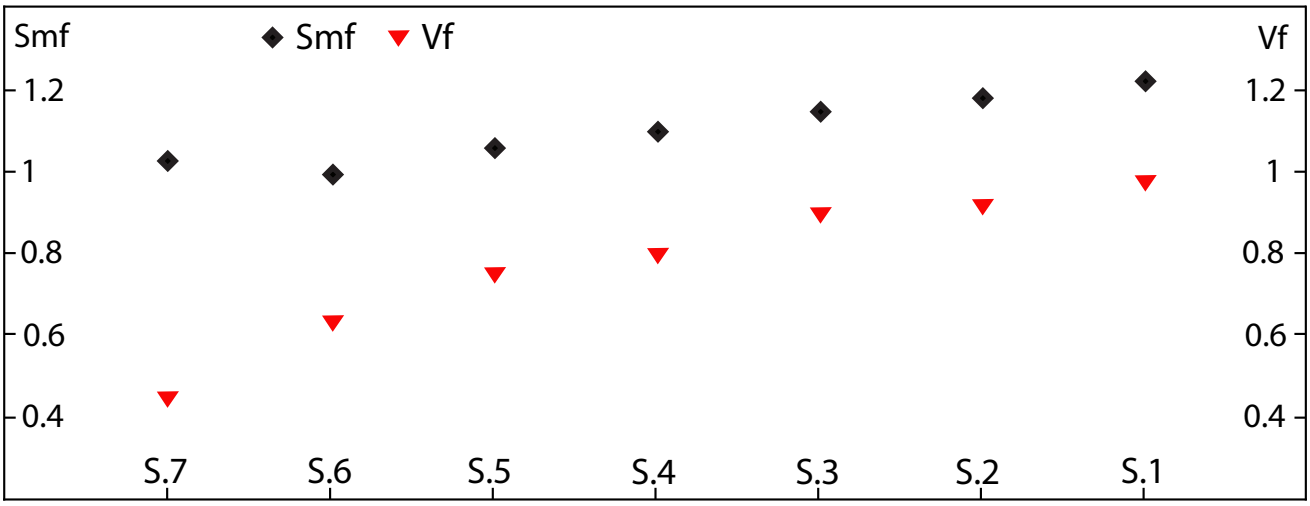

FIGURE 7. Along-strike variations of the S_{mf} and V_f values. Distribution of both values shows close relationship with relief. Low S_{mf} and V_f values are compatible with higher relief and topography hence higher displacement. S.1 through S.7 refer to the fault segments.

35 are symmetric, while catchments 1 and 14 in the central and eastern stretches of the fault are slightly asymmetric. Segments 4 and 5 in the central stretch of the fault have the highest asymmetry values (classes 1 and 2, moderately and strong asymmetry), while the eastern stretch of the fault contains catchments with the lowest asymmetry.

Hypsometric analysis

Most of the catchments have convex and complex HC (Fig. 10A, D). Catchments 4, 15, 16, 22, 26, 28, 32, and 34 have concave HC (Fig. 10B). Catchments 2, 8, 14, 25, and 39 have S-shaped HC (Fig. 10C). The catchments with the convex HC probably have high rate of uplifting. The complex shapes of HC could be due to active continuous erosion at the head and foot of the streams and/or stream piracy events, most probably due to active tectonics in conjunction with lithological control factors (Giaconia *et al.*, 2012). Most segments have catchments with HC ranging from convex to irregular shapes, and HI values ranging from low to intermediate (see methods section for classes; Table 4).

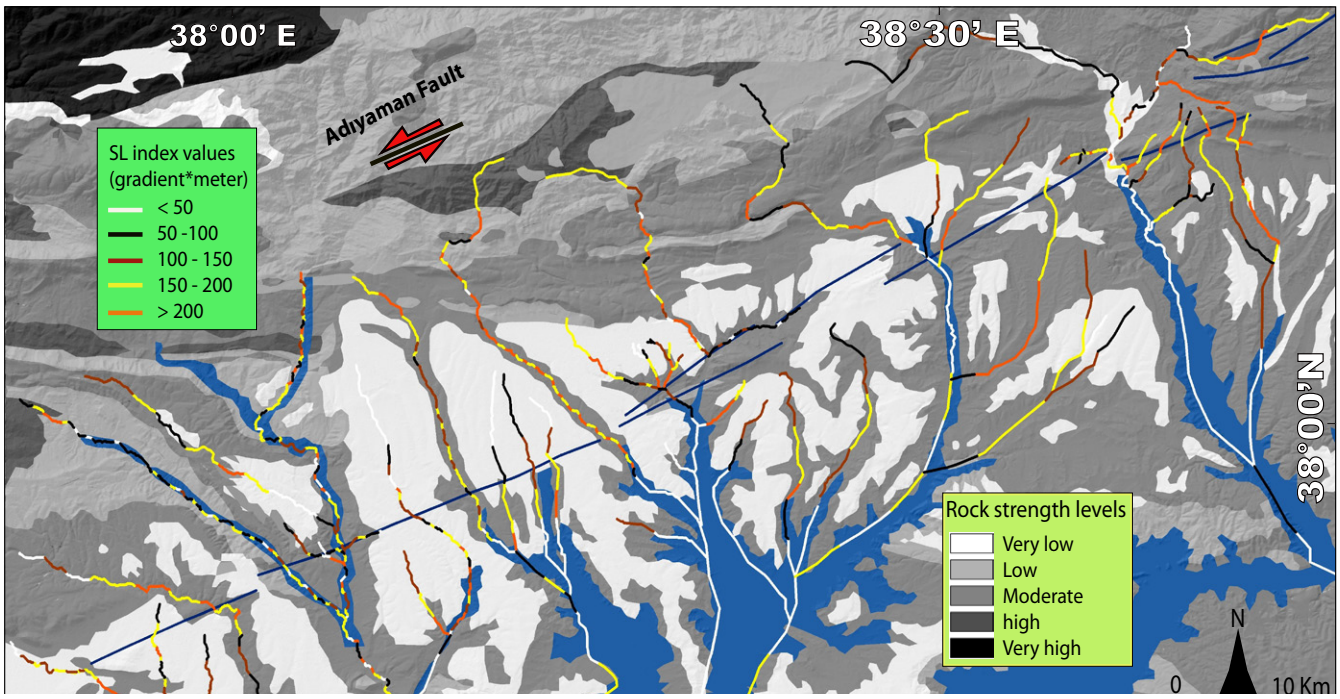

FIGURE 8. S_L indices along the channels and rock strength level (according to Selby, 1980). S_L values increase systematically where they cross the fault segments.

TABLE 3. Asymmetry Factor (AF) values for the catchments within the study area

Catchment No.	AF	AF-50	Class	Catchment No.	AF	AF-50	Class
1	41	-9	3	21	53	3	-
2	82	32	1	22	27	-23	1
3	71	21	1	23	55	5	3
4	51	2	-	24	39	-11	2
5	64	14	2	25	27	-23	1
6	54	4	-	26	47	-3	-
7	51	1	-	27	46	-4	-
8	53	3	-	28	64	14	2
9	27	-23	1	29	54	4	3
10	37	-13	2	30	39	-11	2
11	67	17	1	31	48	-12	2
12	61	11	2	32	46	-4	-
13	33	-17	1	33	86	36	1
14	43	-7	3	34	66	16	1
15	76	26	1	35	47	-3	-
16	67	17	1	36	78	28	1
17	63	13	2	37	39	-11	2
18	27	-23	1	38	33	-17	1
19	70	20	1	39	27	-23	1
20	66	16	1				

Relative Tectonic Activity (RTA)

G_{av} values range from 1.00 to 2.66. Class 1 RTA (high tectonic activity) is mainly concentrated in the middle part of the Adıyaman fault, while the middle part of the eastern and western areas have RTA ranging from class 1 to 2 (intermediate to high tectonic activity). Only catchment 28 in the western part of the Adıyaman fault have a RTA class 3, indicating relatively low tectonic activity (Fig. 11). 61.50–76.60% values of RTA were of class 1, 21.00–35.80% of class 2, and 02.40–02.60% of class 3 (Fig. 12A; B). Averaging of the geomorphic indices classes of the active tectonics G_{av} and values of RTA are summarized in Table 5.

DISCUSSION

The relative motion between the northward movement of the Arabian lithospheric plate and westward movement of the Anatolian lithospheric plate occurs along the EAF

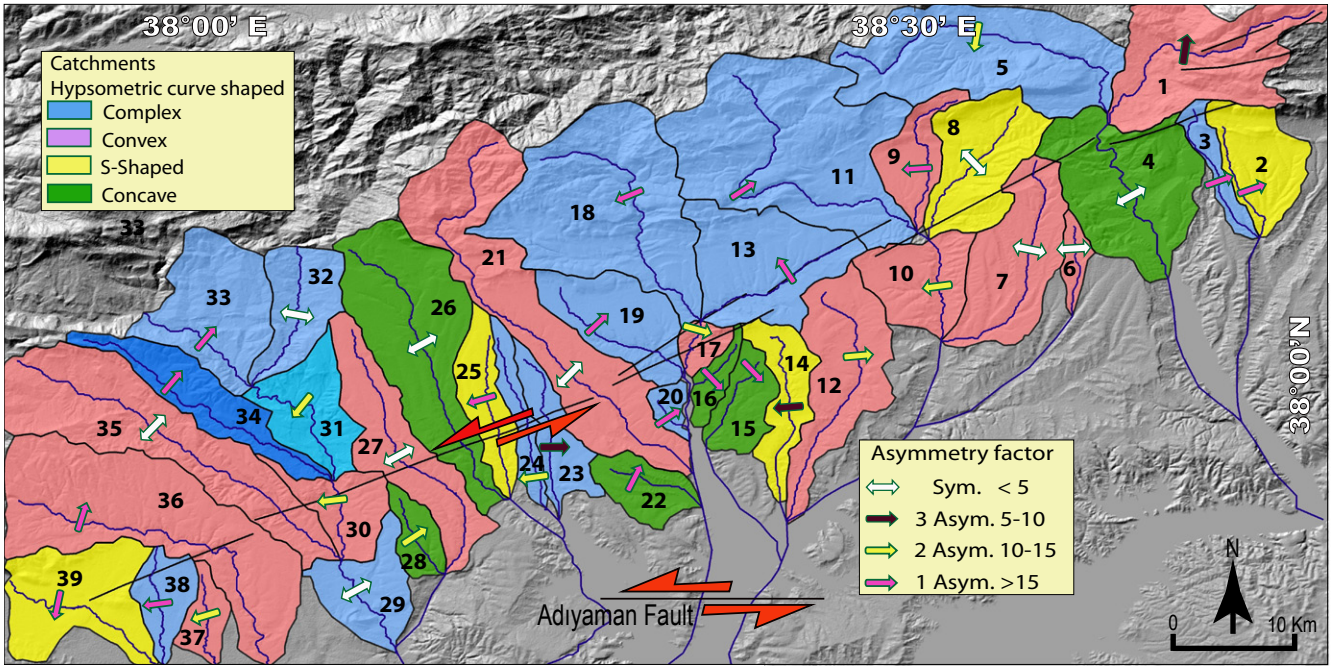

FIGURE 9. Results of the drainage basins/catchments categorized by hypsometric curves shapes and asymmetry factor (AF) values.

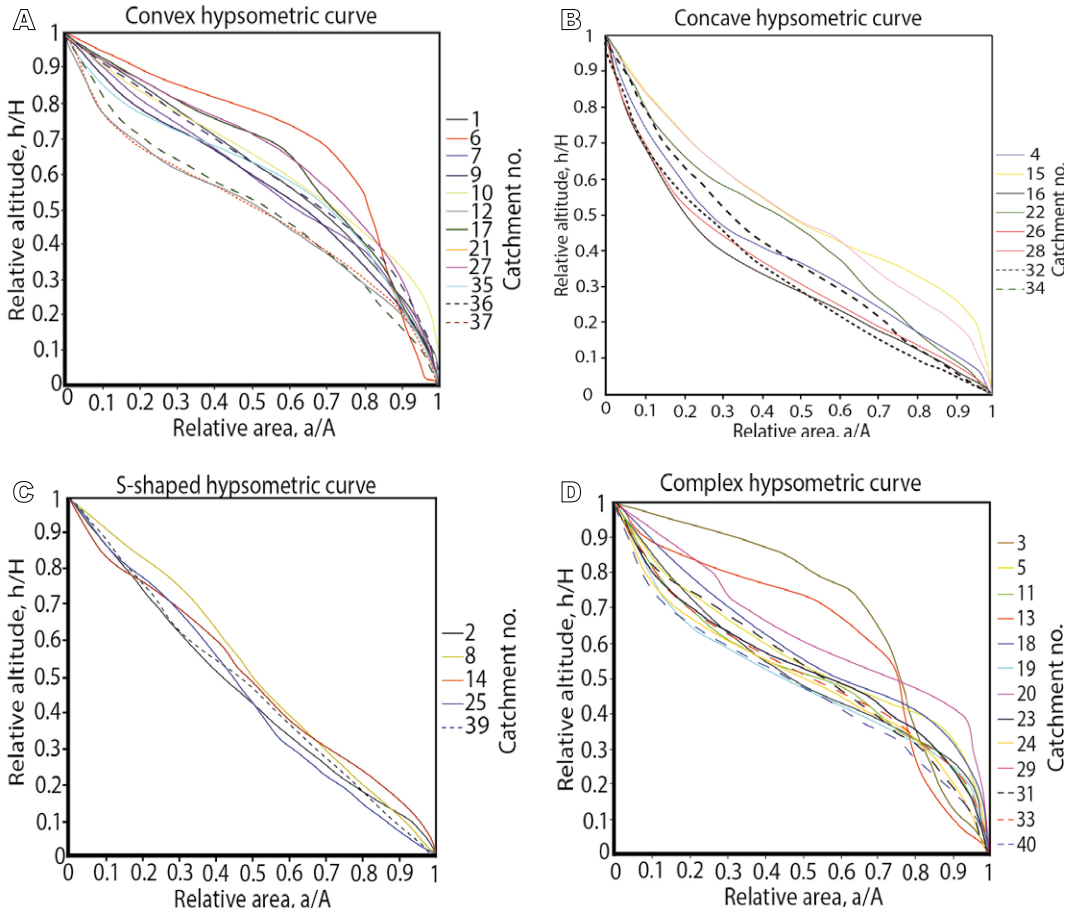

FIGURE 10. Results of the catchments categorized by hypsometric curves shapes (HC). A) HC for weakly eroded basins. B) HC for highly eroded basins. C) HC for moderately eroded basins. D) HC for a basin with stream rejuvenation processes at the foot or head of the stream.

TABLE 4. Hypsometric integral and curves (HI and HC) of the catchments of the study area

Catchment No.	HI	HI Class	HC Class	Catchment No.	HI	HI Class	HC Class
1	0.51	1	1	22	0.24	3	3
2	0.98	1	2	23	0.24	3	-
3	0.28	3	-	24	0.15	3	-
4	0.24	3	3	25	0.36	2	2
5	0.26	3	-	26	0.27	2	3
6	0.31	3	1	27	0.29	3	1
7	0.26	3	1	28	0.28	3	3
8	0.52	1	2	29	0.37	2	-
9	0.34	2	1	30	0.36	1	1
10	0.37	2	1	31	0.45	2	-
11	0.27	3	-	32	0.28	3	3
12	0.38	3	1	33	0.45	2	-
13	0.41	2	-	34	0.23	3	3
14	0.53	1	2	35	0.44	2	1
15	0.40	2	3	36	0.23	3	1
16	0.21	3	3	37	0.39	2	1
17	0.38	2	1	38	0.36	2	-
18	0.26	3	-	39	0.21	3	2
19	0.27	3	-				
20	0.33	2	-				
21	0.29	3	1				

zone in eastern Turkey, with slip rates between 6 and 10mm/yr and a high rate of seismic activity (Aktug *et al.*, 2016). The EAF zone incorporates the Adıyaman fault that parallels the EAF trace. The morphotectonic analysis has been useful to examine the relative tectonic activity of the Adıyaman fault.

In our study, the S_{mf} and V_f chart confirms that all segments of the Adıyaman fault are of class 1 (Fig. 13), which indicates uplift rates <0.5mm/yr (*e.g.* Bull, 2007; Mayer, 1986; Rockwell *et al.*, 1984; Silva *et al.*, 2003). The values of S_{mf} and V_f signify that there is a clear general coherency between them along the whole segments except segment 7 (Table 2; Fig. 7). In the study area, S_L index values generally increase abruptly in the same rock units and record many anomalous points along all fault segments that reflect tectonic signals (Fig. 8). Also, because of mountain-fronts occur along low and very low rock strengths, S_L values confirm that each fault segment is active, with activity to impact the gradients of the channels (Yıldırım, 2014). This supports the view that

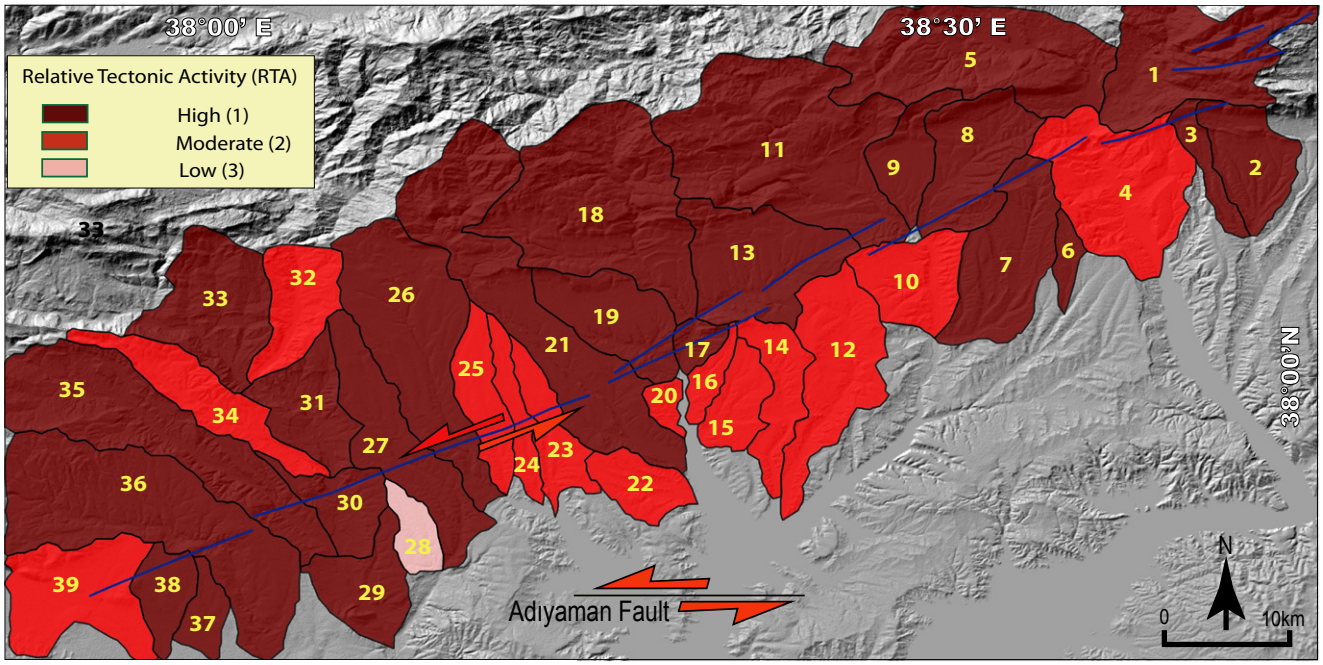

FIGURE 11. Distribution of the Relative Tectonic Activity (RTA) indices along the study fault zone.

the Adıyaman fault is an active fault. The distribution of the geomorphic indices values confirm that the fault segments which are associated with different values of mountain-fronts reflects different rates of RTA (Table 5).

According to the RTA analysis in the study area, about 69.05% of values are of class 1 (high RTA), 28.04% suggests moderate RTA (class 2), and 2.5% shows the lowest values of RTA (class 3). Thus, more than half of

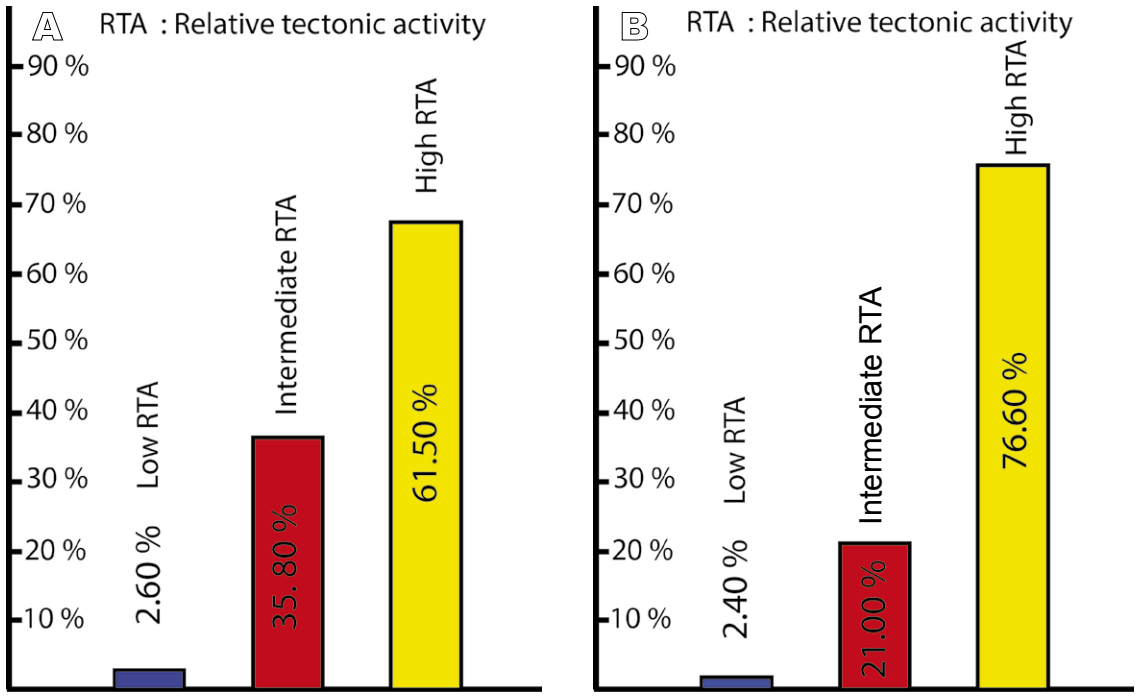

FIGURE 12. The RTA percentage ratios based on A) the catchments numbers and B) based on the catchments areas.

TABLE 5. Classes of Relative Tectonic Activity (RTA) for catchments in the study area (AF: catchment Asymmetry Factor; G_{av}: average of geomorphic indices; HC: hypsometric curves; HI: hypsometric integral).

Catchment No.	HI Class	HC Class	AF Class	G_{av}	RTA Class
1	1	1	3	1.66	1
2	1	2	1	1.33	1
3	3	-	1	1.33	1
4	3	3	-	2.00	2
5	3	-	2	1.66	1
6	3	1	-	1.33	1
7	3	1	-	1.33	1
8	1	2	-	1.00	1
9	2	1	1	1.33	1
10	2	1	2	1.66	2
11	3	-	1	1.33	1
12	3	1	2	2.00	2
13	2	-	1	1.00	1
14	1	2	3	2.00	2
15	2	3	1	2.00	2
16	3	3	1	2.33	2
17	2	1	2	1.66	1
18	3	-	1	1.33	1
19	3	-	1	1.33	1
20	3	3	1	2.33	2
21	2	1	-	1	1
22	3	3	1	2.33	2
23	3	-	3	2.00	2
24	3	-	2	1.66	2
25	2	2	1	1.66	2
26	2	3	-	1.66	1
27	3	1	-	1.33	1
28	3	3	2	2.66	3
29	2	-	3	1.66	1
30	1	1	2	1.33	1
31	2	-	2	1.33	1
32	3	3	-	2.00	2
33	2	-	1	1.00	1
34	3	3	1	2.33	2
35	2	1	-	1	1
36	3	1	1	1.66	1
37	2	1	2	1.66	1
38	2	-	1	1.00	1
39	3	2	1	2.00	2

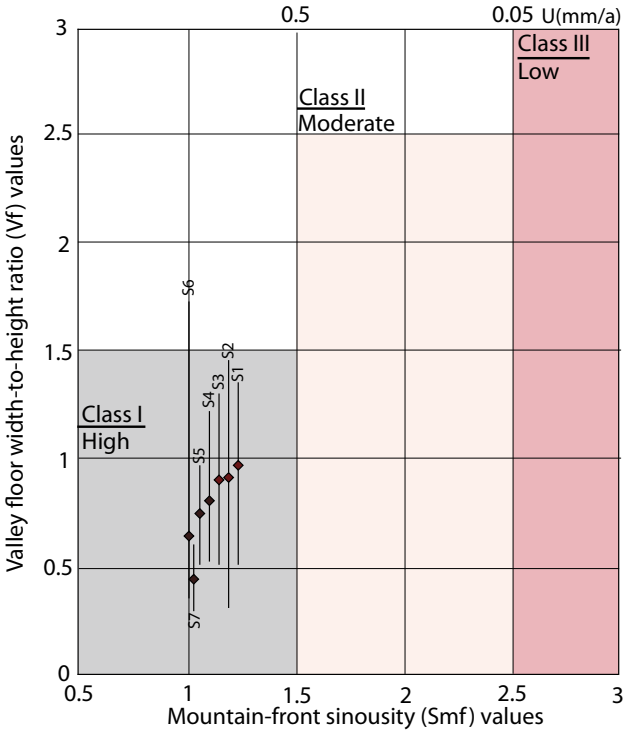

FIGURE 13. The plot of S_{mf} against V_f for the mountain fronts of each segment and inferred activity classes. Vertical bars show the standard deviation (σn-1) for V_f values. Numbers at the top indicate inferred uplift rates U (mm/yr) from Rockwell *et al.* (1984).

the study fault is tectonically highly active in terms of the apparent geomorphic indices values.

In the northern and central regions of Turkey, morphotectonic analysis was applied to define the RTA of faults, including the North Anatolian and Tuz Gölü faults (Selim *et al.*, 2013; Yıldırım, 2014). Selim *et al.* (2013) estimated the morphotectonic indices and confirmed that the southern branch of the North Anatolian fault has RTA classes 1 and 2. The RTA of the Tuz Gölü fault zone in Central Anatolian was examined by Yıldırım (2014) who showed that each segment of the Tuz Gölü fault is highly active (class 1).

Our analysis of the geomorphic indices of the Adıyaman fault suggest that it is an intermediate to high activity fault (Table 5). All fault segments have the highest RTA (class 1) (Table 1; Fig. 13) and the results from G_{av} and RTA analysis indicate moderate to high RTA (classes 1 and 2) along the entire study area. Based on our morphometric analysis, the Adıyaman fault is characterized by shorter recurrence intervals and/or the potential for large earthquakes. Yıldırım (2014) highlighted that most of the seismic risk and hazard investigations concentrate on high-strain regions characterized by destructive earthquakes and high slip-rates. Nonetheless, the recently recorded large earthquakes in continental regions with low-strain and slow slip-rates, *e.g.* Van Lake in Turkey in 2011 (Fielding *et al.*, 2013) suggest that it is important to undertake similar studies in less strained regions, such as in eastern Turkey. The Adıyaman fault, characterized by a high RTA (class 2), poses a significant seismic hazard in the eastern Anatolian region. The March 2, 2017 Adıyaman-Samsat (M_w=5.5) earthquake is an evidence of this view.

The geomorphometric analysis does not directly indicate fault slip rates but helps highlight the potentially strong interaction between faults motion, earthquakes and surface processes that create landforms. Thus, the morphometric studies can provide a very good assessment of the RTA degrees of the fault segments.

In eastern Turkey, the continuing northward drift of the Arabian plate with respect to Eurasia resulted in the Anatolian plate extrusion along the North and EAF (Şengör *et al.*, 2005). The sinistral strike-slip EAF zone represents the main transform structure in this area. The EAF zone comprises some pure transform strike-slip faults that are parallel to the motion between Arabian and Anatolian lithospheric plates, where other faults are oblique to the plate motion (Bozkurt, 2001). The EAF zone is very complex region that contains many pull-apart basins (Hempton *et al.*, 1981), as well as folded and thrusted units (Arpat and Şaroğlu, 1972). The seismicity was observed along ~20–30km-wide zone along strike of the EAF (Bulut *et al.*, 2012). The seismicity of the EAF zone that records large destructive earthquakes, *e.g.* May 22, 1971 Bingöl (M_w=6.6) earthquake indicates a high rate of tectonic activity along the main trace of the fault (Ambraseys, 1989). Bulut *et al.* (2012) suggested a systematic migration of moderate and micro-size (M_w=2.5–5.5) earthquakes from the main EAF into adjacent faults confirming progressive interaction between the major trend of the EAF zone and its secondary structures. However, the RTA results of Adıyaman fault that offer a moderate tectonic activity rate, suggest that it is of secondary importance compared to the EAF zone in accommodating the regional deformation of Anatolia. This is consistent with GPS studies (Aktuğ *et al.*, 2016; Reilinger *et al.*, 2006) that show most displacement is occurring across the EAF as compared to the Adıyaman fault.

CONCLUSION

Quantitative geomorphic indices provide important clues about the effects of active tectonics. The relationship between values of S_{mf} with V_f, and S_L and the average combination of other geomorphic indices including HI, HC, and AF, provide evidences of the activity of the Adıyaman

fault. The fault is divided into three classes of RTA based on G_{av} values. The entire fault is moderately to highly active, classes 2 and 3, based on the RTA analysis. The more active tectonic areas are concentrated in the middle and eastern parts of the fault, segments 2, 4, 5, and 6. Similarly, the western stretches of the fault have a high degree of RTA, while the eastern part indicates moderate to high degree of tectonics. The values of S_{mf}, V_f, and S_L with RTA values in the central and western stretches of the fault likely reflect a higher seismic risk with respect to the eastern parts of the fault zone. In eastern Turkey, the motion between the Arabian and Anatolian lithospheric plates resulted in the formation of the active East Anatolian strike-slip fault with secondary parallel strike-slip faults such as Adıyaman fault. The linear indices and RTA analysis suggest that the Adıyaman fault is of secondary importance compared to the EAF in accommodating the relative motion between the Arabian and Anatolian lithospheric plates.

ACKNOWLEDGMENTS

This research has been funded by Istanbul Technical University BAP project. PhD. scholarship to A. Khalifa from the Turkish Government (YTB) in cooperation with the Egyptian Government (Cultural Affairs and Mission Sector) is acknowledged. The PhD candidate A. Khalifa was hosted as a visitor student in University of Cincinnati for one year, the support from the Department of Geology in the University of Cincinnati is appreciated. We thank the editor and referees for their constructive comments and advice that greatly helped us to improve our manuscript.

REFERENCES

Aksoy, E., İnceöz, M., Koçyiğit, A., 2007. Lake Hazar Basin: a Negative Flower Structure on the East Anatolian Fault System (EAFS), SE Turkey. Turkish Journal of Earth Science, 16(3), 319-338.

Aktuğ, B., Özener, H., Dogru, A., Sabuncu, A., Turgut, B., Halicioglu, K., Yilmaz, O., Havazli, E., 2016. Slip rates and seismic potential on the East Anatolian Fault System using an improved GPS velocity field. Journal of Geodynamics, 94-95, 1-12.

Alipoor, R., Poorkermani, M., Zare, M., El Hamdouni, R., 2011. Active tectonic assessment around Rudbar Lorestan dam site, High Zagros Belt (SW of Iran). Geomorphology, 128(1-2), 1-14.

Allen, C.R., 1969. Active Faulting in Northern Turkey. Division of Geological Science Contribution, California Institute of Technology Contribution, 1577, 32pp.

Ambraseys, N.N., 1989. Temporary seismic quiescence: SE Turkey. Geophysics Journal International, 96(2), 411-431.

Arpat, E., Şaroğlu, F., 1972. The East Anatolian Fault System: thoughts on its development. The Mineral Research and Exploration Institute of Turkey (MTA), 78, 33-39.

Azor, A., Keller, E.A., Yeats, R.S., 2002. Geomorphic indicators of active fold growth: South Mountain–Oak Ridge anticline, Ventura basin, southern California. Geological Society of America Bulletin, 114(6), 745-753.

Barka, A.A., Şaroğlu, F., Güner, Y., 1983. Horasan-Narman depremi ve bu depremin Doğu Anadolu neotektonigindeki yeri. Yeryuvan Ve Insan, 8(3), 16-21. [In Turkish with English abstract] [Available in: https://www.jmo.org.tr/resimler/ekler/fcf34635f905065_ek.pdf?dergi=YERYUVARI%20VE%20%DDNSAN]

Bozkurt, E., 2001. Neotectonics of Turkey – a synthesis. Geodinamica Acta, 14(1-3), 3-30.

Bull, W.B., McFadden, L.D., 1977. Tectonic geomorphology north and south of the Garlock Fault, California. In: Doehering, D.O. (ed.). Geomorphology of Arid Regions. Binghamton, State University of new York, proceedings of the 8th Annual Geomorphology Symposium Proceedings, 115-138.

Bull, W.B., 2007. Tectonic Geomorphology of Mountains: A new Approach to Paleoseismology. Hoboken, New Jersey, USA, Wiley - Blackwell, 328pp.

Bulut, F., Bohnhoff, M., Eken, T., Janssen, C., Kılıç, T., Dersen, G., 2012. The East Anatolian Fault Zone: Seismotectonic setting and spatiotemporal characteristics of seismicity based on precise earthquake locations. Journal of Geophysical Research, 117(B7), 1-16.

Canıtez, N., Üçer B., 1967. A catalogue of focal mechanism diagrams for Turkey and adjoining areas. Istanbul Technical University Arz. Fizigi Enstitusu, 25.

Chen, Y.C., Sung, Q., Cheng, K.-Y., 2003. Along-strike variations of morphotectonic features in the Western Foothills of Taiwan: tectonic implications based on stream-gradient and hypsometric analysis. Geomorphology, 56(1-2), 109-137.

Ciccacci, S., D'Alessandro, L., Fredi, P., Lupia-Palmeri, E., 1992. Relations between morphometric characteristics and denudational processes in some drainage basins of Italy. Zeitschfirt für Geomorphologie, 36, 53-67.

D'Alessandro, L., Del Monte, M., Fredi, P., Lupia-Palmeri, E., Peppoloni, S., 1999. Hypsometric Analysis in the Study of Italian Drainage Basin Morphoevolution. Transactions, Japanese Geomorphological Union, 20(3), 187-202.

Dewey, J.F., Hempton, M.R., Kidd, W.S.F., Şaroğlu, F., Şengör, A.M.C., 1986. Shortening of continental lithosphere: the neotectonics of Eastern Anatolia-a young collision zone. In: Coward, M.O., Ries, A.C. (eds.). Collisional Tectonics. Geological Society, London, Special Publication, 19(1) 3-36.

Dumont, J.F., Santana, E., Vilema, W., 2005. Morphologic evidence of active motion of the Zambapala Fault, Gulf of Guayaquil (Ecuador). Geomorphology, 65(3-4), 223-239.

El Hamdouni, R., Irigaray, C., Fernández, T., Chacón, J., Keller, E.A., 2008. Assessment of relative active tectonics, southwest border of the Sierra Nevada (southern Spain). Geomorphology, 96(1-2), 150-173.

Eyidoğan, H., Nalbant S.S., Barka A.A., King G.C.P., 1999. Static stress changes induced by the 1924 Pasinler (M=6.8) and

1983 Horasan-Narrnan (M=6.8) earthquakes, Northeastern Turkey. Terra Nova, 11(1), 38-44.

Farr, T.G., Rosen, P.A., Caro, E., Crippen, R., Duren, R., Hensley, S., Kobrick, M., Paller, M., Rodriguez, E., Roth, L., Seal, D., Shaffer, S., Shimada, J., Umland, J., Werner, M., Oskin, M., Burbank, D., Alsdorf, D., 2007. The Shuttle Radar Topography Mission. Reviews of Geophysics, 45(2), 1-33.

Fielding, E.J., Lundgren, P.R., Taymaz, T., Yolsal-Çevikbilen, S., Owen, S.E., 2013. Fault-slip sourcemodels for the 2011 M7.1 Van earthquake in Turkey from SAR interferometry, pixel offset tracking, GPS and seismic waveform analysis. Seismological Research Letters, 84(4), 579-593.

Frank, P., Claudio, B., Ryan ,M., Kellen, G., Alese, K., 2011. Tectonic geomorphology and Earth Scope in Eastern North America. Abstract. Minneapolis, GSA Annual meeting in Minneapolis, 9-12 October, 43, 5, 363.

Giaconia, F., Booth-Rea, G., Martínez-Martínez, J.M., Azañón, J.M., Pérez-Peña, J.V., 2012. Geomorphic analysis of the Sierra Cabrera, an active pop-up in the constrictional domain of conjugate strike-slip faults: The Palomares and Polopos fault zones (eastern Betics, SE Spain). Tectonophysics, 580, 27-42.

Giamboni, M., Wetzel, A., Schneider, B., 2005. Geomorphic response of alluvial rivers to active tectonics: example from the southern Rhinegraben. Australian Journal of Earth Sciences, 97, 24-37.

Gordon, R.G., 1998. The plate tectonic approximation: plate nonrigidity, diffuse plate boundaries, and global plate reconstructions. Annual review of Earth and Planteary Sciences, 26(1), 615-642.

Hack, J.T., 1973. Stream-profiles analysis and stream-gradient index. Journal of Research of the U.S. Geological Survey, 1(4), 421-429.

Hare, P.H., Gardner, T.W., 1985. Geomorphic indicators of vertical neotectonism along the converging plate margins, Nicoya Peninsula, Costa Rica. In: Morisawa, M., Hack, J.T. (eds.). Allen and Unwin, Boston, MA, Tectonic Geomorphology, 4, 75-104.

Hempton, M.R., Dewey, J.F., Şaroğlu, F., 1981. The East Anatolian transform fault: along strike variations in geometry and behaviour. EOS Transactions American Geophysical Union, 62, 393.

Hempton, M.R., 1987. Constraints on Arabian Plate motion and extensitonal history of the Red Sea. Tectonics, 6(6), 687-705.

Herece, E., 2008. Atlas of the East Anatolian Fault, General Directorate of Mineral Research and Exploration (MTA), Special Publication Series, 13.

Keller, E.A., Printer, N., 2002. Active Tectonics. Earthquakes, Uplift and Landscape. New Jersey, Prentice Hall, 362pp.

Khalifa, A., Çakir, Z., Owen L.A., Kaya, Ş., 2018. Morphotectonic analysis of the East Anatolian Fault, Turkey. Turkish Journal of Earth Sciences, 27, 110-126.

Lifton, N.A., Chase, C.G., 1992. Tectonic, climatic and lithologic influences on landscape fractal dimension and hypsometry: implications for landscape evolution in the San Gabriel Mountains, California. Geomorphology, 5(1-2), 77-114.

Mahmood, S.A., Gloaguen, R., 2012. Appraisal of active tectonics in Hindu Kush: Insights from DEM derived geomorphic indices and drainage analysis. Geoscience Frontiers, 3(4), 407-428.

Matoš, B., Pérez-Peña, J. V., Tomljenovi, B., 2016. Landscape response to recent tectonic deformation in the SW Pannonian Basin: Evidences from DEM-based morphometric analysis of the Bilogora Mt. area, NE Croatia. Geomorphology, 263, 132-155.

Mayer, L., 1986. Tectonic Geomorphology of Escarpments and Mountain fronts. Active Tectonics, 7, 125-135.

McKenzie, D., 1972. Active Tectonics of the Mediterranean Region. Geophysical Journal International, 30(2), 109-185. DOI: 10.1111/j.1365-246X.1972.tb02351.x

Molin, P., Pazzaglia, F.J., Dramis, F., 2004. Geomorphic expression of active tectonics in a rapidly-deforming forearc, Sila massif, Calabria, southern Italy. American Journal of Science, 304(7), 559-589.

Necea, D., Fielitz, W., Matenco, L., 2005. Late Pliocene–Quaternary tectonics in the frontal part of the SE Carpathians: Insights from tectonic geomorphology. Tectonophysics, 410(1-4), 137-156.

Ohmori, H., 1993. Changes in the hypsometric curve through mountain building resulting from concurrent tectonics and denudation. Geomorphology, 8(4), 263-277.

Pérez-Peña, J.V., Azor, A., Azañón, J.M., Keller, E.A., 2010. Active tectonics in the Sierra Nevada (Betic Cordillera, SE Spain): Insights from geomorphic indices and drainage pattern analysis. Geomorphology, 119(1-2), 74-87.

Perinçek, D., Çemen, İ., 1990. The structural relationship between the East Anatolian and Dead Sea fault zones in Southeastern Turkey. Tectonophysics, 172(3-4), 331-340.

Reilinger, R., McClusky, S., Vernant, P., Lawrence, S., Ergintav, S., Cakmak, R., Ozener, H., Kadirov, F., Guliev, I., Stepanyan, R., Nadariya, M., Hahubia, G., Salah, M., Sakr, K., ArRajehi, A., Paradissis, D., Al-Aydrus, A., Prilepin, M., Guseva, T., Evren, E., Dmitrotsa, A., Filikov, S.V., Gomez, F., Al-Ghazzi, R., Gebran, K., 2006. GPS constraints on continental deformation in the Africa-Arabia–Eurasia continental collision zone and implications for dynamics of plate interactions. Journal of Geophysical Research Solid Earth, 111(B5), 1-26.

Rockwell, T.K., Keller, E.A., Johnson, D.L., 1984. Tectonic geomorphology of alluvial fans and mountain fronts near Ventura, California. In: Morisawa, M., Hack, J.T. (eds.). Tectonic Geomorphology. Allen and Unwin, Boston, MA, Proceedings of the 15th Annual Geomorphology Symposium, 183-207.

Selçuk, S.A., 2016. Evaluation of the relative tectonic activity in the eastern Lake Van basin, East Turkey. Geomorphology, 270, 9-21.

Selby, M.J., 1980. A rock strength classification for geomorphic purposes: with tests from Antarctica and New Zealand. Z. Geomorphlogi, 24, 21-51.

Selim, H.H., Tüysüz, O., Karakaş, A., Taş, K.Ö., 2013. Morphotectonic evidence from the southern branch of

the North Anatolian Fault (NAF) and basins of the south Marmara sub-region, NW Turkey. Quaternary International, 292, 176-192.

Silva, P.G., Goy, J.L., Zazo, C., Bardajı, T., 2003. Fault-generated mountain fronts in southeast Spain: geomorphologic assessment of tectonic and seismic activity. Geomorphology, 50(1-3), 203-225.

Strahler, A.N., 1952. Hypsometric (area-altitude) analysis of erosional topography. The Geological Society of America Bulletin, 63(11), 1117-1142.

Şaroğlu F., Emre Ö., Kuşçu İ., 1992. Active Fault Map of Turkey. General Directorate of Mineral and Research Exploration of Turkey (MTA) Publication, Ankara, Turkey.

Şengör, A.M.C., Görür, N., Şaroğlu, F., 1985. Strike-slip faulting and related basin formation in zones of tectonic escape: Turkey as a case study. In: Biddle, K.T., Christie-Slick N. (eds.). Strike-slip Faulting and Basin Formation. Society of Economic Paleontologist and Mineralogists, Tulsa, Special Publication, 37, 227-264.

Şengör, A.M.C., Tüysüz, O., İmren, C., Sakınç, M., Eyidoğan, H., Görür, N., Le Pichon, X., Rangin, C., 2005 The North Anatolian Fault: A new look. Annual review of earth and planetary science, 33, 37-112.

Taymaz, T., Jackson, J., McKenzie, D.P., 1991. Active tectonics of north and central Aegean Sea. Geophysical Journal International, 106(2), 433-490.

Toksöz, M.N., Guenette, M., Gülen, L., Keough, G., Pulli, J.J., Sav, H., Olguner, A., 1983. 30 Ekim 1983 Narman-Horasan depreminin kaynak mekaniszmasi Yeryuvan Ve Insan 8(3), 47-52 [In Turkish with English abstract][Available in: https://www.jmo.org.tr/resimler/ekler/a7bd93c6f3112cb_ek.pdf?dergi=YERYUVARI%20VE%20%DDNSAN]

Tsodoulos, I.M., Koukouvelas, I.K., Pavlides, S., 2008. Tectonic geomorphology of the easternmost extension of the Gulf of Corinth (Beotia, Central Greece). Tectonophysics, 453(1-4), 211-232.

Ul-Hadi, S., Shuhab, D.K., Lewis, A.O., Abdul, S.K., 2013. Geomorphic response to an active transpressive regime: a case study along the Chaman strike-slip fault, western Pakistan. Earth Surface Processes and Landforms, 38(3), 250-264.

Wells, S.G., Bullard, T.F., Menges, C.M., Dark, P.G., Keras, P.A., Kelson, K.I., Ritter, J.B., Wesling, J.R., 1988. Regional variations in tectonic geomorphology along a segmented convergent plate boundary pacific coast of Costa Rica. Geomorphology, 1(3), 239-265.

Westaway, R., 1994. Present-day kinematics of the Middle East and eastern Mediterranean. Journal of Geophysical Research, 99(B6), 12071-12090.

Willgoose, G., 1994. A physical explanation for an observed area-slope–elevation relationship for catchments with declining relief. Water Resources Research, 30(2), 151-159.

Willgoose, G., Hancock, G., 1998. Revisiting the hypsometric curve as an indicator of form and process in transport-limited catchment. Earth Surface Processes and Landforms, 23(7), 611-623.

Yıldırım, C., 2014. Relative tectonic activity assessment of the Tuz Gölü Fault Zone; Central Anatolia, Turkey. Tectonophysics, 630, 183-192.

Manuscript received July 2017;
revision accepted March 2019;
published Online June 2019.